HHS Public Access

Author manuscript

Nat Cell Biol. Author manuscript; available in PMC 2015 October 01.

Published in final edited form as:

Nat Cell Biol. 2014 October ; 16(10): 931–8. doi:10.1038/ncb3036.

Endothelial podosome rosettes regulate vascular branching in tumour angiogenesis

Giorgio Seano[1,2,3,9], **Giulia Chiaverina**[1,2], **Paolo Armando Gagliardi**[1,2], **Laura di Blasio**[1,2], **Alberto Puliafito**[1,2], **Claire Bouvard**[4,8], **Roberto Sessa**[1,2,8], **Guido Tarone**[5], **Lydia Sorokin**[6], **Dominique Helley**[7], **Rakesh K. Jain**[3], **Guido Serini**[1,2], **Federico Bussolino**[1,2], and **Luca Primo**[1,2,9]

[1]Department of Oncology, University of Torino, Turin 10100, Italy

[2]Candiolo Cancer Institute-FPO, IRCCS, Candiolo 10060, Italy

[3]Edwin L. Steele Laboratory for Tumor Biology, Harvard Medical School, Massachusetts General Hospital, Boston, Massachusetts 02114, USA

[4]UMR-S 765, Université Paris Descartes, Sorbonne Paris Cité, Paris 75006, France

[5]Department of Molecular Biotechnology and Health Sciences, University of Torino, Molecular Biotechnology Center, Turin 10124, Italy

[6]Institute of Physiological Chemistry and Pathobiochemistry, Muenster University, Muenster 48149, Germany

[7]UMR-S 970, Université Paris Descartes, Sorbonne Paris Cité, Paris 75006, France

Abstract

The mechanism by which angiogenic endothelial cells break the physical barrier of the vascular basement membrane and consequently sprout to form new vessels in mature tissues is unclear. Here, we show that the angiogenic endothelium is characterized by the presence of functional podosome rosettes. These extracellular-matrix-degrading and adhesive structures are precursors of *de novo* branching points and represent a key feature in the formation of new blood vessels. VEGF-A stimulation induces the formation of endothelial podosome rosettes by upregulating integrin $\alpha_6\beta_1$. In contrast, the binding of $\alpha_6\beta_1$ integrin to the laminin of the vascular basement membrane impairs the formation of podosome rosettes by restricting $\alpha_6\beta_1$ integrin to focal adhesions and hampering its translocation to podosomes. Using an *ex vivo* sprouting angiogenesis

[9]Correspondence should be addressed to G.S. or L.P. (seano@steele.mgh.harvard.edu or luca.primo@ircc.it).

[8]Present addresses: The Scripps Research Institute, La Jolla, California 92037, USA (C.B.); Center for Eye Disease and Development, University of California, Berkeley, California 94720, USA (R.S.)

Note: Supplementary Information is available in the online version of the paper

AUTHOR CONTRIBUTIONS

G Seano and L.P. conceived the idea and wrote the manuscript; G Seano, G.C., P.A.G, A.P. and L.d.B. performed the experiments and analysed the data; L.S. provided LAMA4 mARs; C.B. and D.H. provided endothelial α_6 null mARs, B16F10 tumours and ischaemic tissues; R.K.J. provided human samples; G. Serini, G.T., R.K.J. and FB. analysed and discussed the data; all authors reviewed and approved the manuscript.

COMPETING FINANCIAL INTERESTS

The authors declare no competing financial interests.

assay, transgenic and knockout mouse models and human tumour sample analysis, we provide evidence that endothelial podosome rosettes control blood vessel branching and are critical regulators of pathological angiogenesis.

Angiogenesis, the development of new vessels from pre-existing ones, plays a critical role in cancer progression. Endothelial cells (ECs), which lead this process, need to overcome several mechanisms attempting to keep the vascular network quiescent. To sprout and form new vessels, the first barrier that ECs have to cross is the vascular basement membrane (vBM), composed of laminins, collagen and proteoglycans[1].

Angiogenic factors, such as the well-studied vascular endothelial growth factor[2–4] (VEGF), guide sprouting angiogenesis. When quiescent vessels sense angiogenic signals, tip ECs are stimulated to invade the underlying layer of vBM that prevents sprouting. This process requires proteolytic breakdown of selected vBM proteins that can be mediated by matrix metalloproteases (MMPs), such as membrane type-1 MMP (MT1-MMP; refs 5,6). However, the cellular mechanisms required for this process remain largely unknown.

Podosomes and invadopodia, collectively called invadosomes, are specialized cell–matrix contacts with an inherent ability to degrade extracellular matrix (ECM) in restricted areas and are typically characterized by enrichment in F-actin and cortactin[7–9]. They are considered key structures of cells that are able to cross anatomical boundaries, such as monocyte-derived cells and transformed fibroblasts[7,10]. Cultured ECs contain either isolated 1-μm-wide individual podosomes or 4–8-μm-wide ring-like clusters of podosomes, called podosome rosettes[7,11,12]. The appearance of individual podosomes and rosettes in ECs can be increased by soluble factors, such as TGF-β, or by phorbol esters[11,12]. Although endothelial podosome rosettes have been observed in TGF-β-stimulated aortic explants[11], definitive *in vivo* evidence for their existence and a functional role for such structures is still lacking.

Here, we show that endothelial rosettes are critical regulators of sprouting angiogenesis and control tumour blood vessel branching. We demonstrate how the VEGF-induced upregulation of the α_6 integrin subunit in ECs induces the formation of podosome rosettes and overcomes the vascular stabilizing and anti-angiogenic effects of the vBM laminin.

RESULTS

VEGF-A induces the assembly of podosome rosettes in ECs

Podosomes (identified by the co-localization of F-actin/cortactin at the basal side of ECs) were organized in two different structures: individual podosomes or multiple podosomes clustered into podosome rosettes[7,11,12] (Fig. 1a). Both structures were rarely present in cultured ECs but their amount can be increased with phorbol-12-myristate-13-acetate (PMA) treatment[12,13] (Fig. 1a). We evaluated whether the number of cells carrying individual podosomes or podosome rosettes was altered in angiogenic endothelium by comparing ECs that were previously stimulated or not with VEGF-A for 24 h. The number of podosome-rosette-containing ECs gradually increased over time and was significantly higher in angiogenic than in quiescent ECs (Fig. 1b and Supplementary Fig. 1a,b).

Conversely, the number of ECs carrying individual podosomes was not influenced (Fig. 1b). Moreover, we observed self-organizing podosome rosettes in angiogenic LifeAct–RFP-transduced[14] ECs (Supplementary Video 1).

As MT1-MMP is considered the main ECM proteinase in podosomes[7,15,16], we quantified the active form of MT1-MMP by flow cytometry. The amount of active MT1-MMP in angiogenic ECs gradually increased during PMA treatment (Supplementary Fig. 1c) and, after 40 min, it was 1.8-fold higher in angiogenic compared with quiescent ECs (Fig. 1c). Moreover, larger areas of gelatin degradation—previously associated with podosomes[13]—were present in cells with podosome rosettes compared with individual podosomes (Fig. 1d).

To investigate whether endothelial podosome rosettes were present not only in cultured angiogenic ECs but also in vascular angiogenic endothelium, we analysed mouse aortic explants *ex vivo*-treated with VEGF-A for 48h (Supplementary Fig. 1d). VEGF-A-stimulated aortae exhibited podosome rosettes, identified as circular F-actin-and cortactin-containing structures localized on the basal side of the endothelial layer (Fig. 1e and Supplementary Fig. 1d,e). In agreement with our *in vitro* observation, the number of cells with rosettes significantly increased in the endothelial layer of VEGF-A-stimulated aortae compared with unstimulated samples (Fig. 1f).

Tumour angiogenic vessels are characterized by high levels of functional endothelial podosome rosettes

To investigate the presence of podosome rosettes in adult vessels undergoing *in vivo* angiogenesis, we analysed several tissues: two mouse models of tumour angiogenesis—the xenograft of B16F10 melanoma[17] and the RipTag2 genetic modelofpancreatic insulinoma[3]; a mouse model of post-ischaemic angiogenesis—the hindlimb ischaemia on gastrocnemius muscles[18,19]; and human clinical biopsies from lung tumours where high vascularity correlates with tumour progression[20]. In all tissues we were able to detect F-actin- and cortactin-positive ring-like structures in the EC membrane in close contact with vBM (Fig. 2a and Supplementary Fig. 2a – c). Notably, F-actin/cortactin rings were characterized by the absence or reduction of laminin staining in vBM (Fig. 2a and Supplementary Fig. 2d). This suggests that vBM components could be locally degraded. Indeed, *in situ* zymography[21] on RipTag2 tumour slices revealed gelatinase activity in the regions that contained F-actin ring-like structures and were simultaneously devoid of laminin staining (Fig. 2b and Supplementary Fig. 2e,f). Podosome rosettes in tumour and ischaemic vessels had a mean diameter of (2.7 ± 0.7) μm (Fig. 2a and Supplementary Fig. 2c) and revealed the presence of podosomal markers, such as dynamin, phospho-FAK, phospho-cortactin and MT1-MMP (Supplementary Fig. 3a).

RipTag2 mice tumours are characterized by an angiogenic switch phase[3,22]. We visualized and quantified the number of endothelial podosome rosettes in tumour vasculature at different stages of tumour progression (Fig. 2c and Supplementary Fig. 3b). Whereas quiescent capillaries of normal islets were characterized by a negligible level of rosettes, the density of rosettes was strongly and significantly increased during the transition from the hyperplastic to the *in situ* tumour stage (Fig. 2c). Moreover, by measuring podosome rosettes in human lung tumour biopsies, we found that endothelial podosome rosette density

is correlated with microvessel density and VEGF-A quantity (Fig. 2d,e and Supplementary Fig. 3c). Therefore, it seems that tumour angiogenic endothelium is characterized by a high number of ECM-degrading podosome rosettes.

$\alpha_6\beta_1$ integrin is essential for VEGF-induced endothelial podosome rosettes

Integrins are known to be involved in podosome formation[7,16,23–25]. Most of the integrins expressed in ECs were recruited in podosome rosettes of angiogenic ECs (Fig. 3a and Supplementary Fig. 4a). To investigate whether these integrins are functionally implicated in rosette formation, we treated angiogenic ECs with specific function blocking antibodies. The inhibition of $\alpha_1\beta_1$, $\alpha_2\beta_1$, $\alpha_4\beta_1$, $\alpha_6\beta_1$ or $\alpha v\beta_3$ significantly impaired podosome rosette formation, suggesting a specific role for these integrins in rosette dynamics. Notably, only the $\alpha_6\beta_1$ inhibition completely blocked the VEGF-induced rosette formation (Fig. 3a,b), impairing, in turn, MT1-MMP membrane localization and gelatin degradation (Fig. 3c and Supplementary Fig. 4b). Interestingly, individual podosomes were not affected by the anti-$\alpha_6\beta_1$ treatment (Supplementary Fig. 4c). We confirmed the $\alpha_6\beta_1$ involvement in rosette formation by silencing the α_6 subunit (Supplementary Fig. 4d). Angiogenic ECs with reduced $\alpha_6\beta_1$ integrin levels failed to form podosome rosettes (Fig. 3d). Furthermore, consistent with previous results[26,27], VEGF stimulation strongly upregulated the expression of α_6 integrin in ECs (Supplementary Fig. 4e), thus pointing to $\alpha_6\beta_1$ as a potential effector acting downstream of VEGF in the signalling pathway that drives rosette formation.

Integrin $\alpha_6\beta_1$ was gradually recruited in podosome rosettes during their formation (Supplementary Fig. 5a); we therefore speculated that $\alpha_6\beta_1$ levels in endothelial podosome rosettes could correlate with their stability. To test this hypothesis, we analysed the lifespan of podosomes composing the rosettes in integrin α_6–GFP (α_6–GFP) and LifeAct– RFP-expressing ECs. Podosomes with high levels of integrin $\alpha_6\beta_1$ exhibited significantly longer lifespans than podosomes with low $\alpha_6\beta_1$ integrin (Fig. 3e and Supplementary Fig. 5b), confirming a crucial role for integrin α_6 in the stability of podosomes in rosettes.

We then analysed α_6 localization in VEGF-A-stimulated aortic explants. Integrin α_6 co-localized with F-actin/cortactin ring-like structures in the basal side of the endothelial layer (Fig. 3f and Supplementary Fig. 5c), and lentiviral-mediated downregulation of α_6 integrin in whole aortic explants significantly impaired rosette formation (Supplementary Fig. 5d). Moreover, experiments with aortic explants from Tie2-dependent integrin α_6 null mice[19] showed that genetic ablation of endothelial α_6 completely suppressed the formation of endothelial rosettes (Fig. 3g).

Laminin impairs endothelial podosome rosette formation

To gain insight into the function of $\alpha_6\beta_1$ integrin in rosette formation, we investigated the role of laminin, the main $\alpha_6\beta_1$ ligand[26]. Unexpectedly, plating ECs on laminin severely inhibited VEGF-A-induced rosette formation and strongly decreased the level of active MT1-MMP (Fig. 4a,b), but did not reduce the number of individual podosomes (Supplementary Fig. 6a). On the basis of these observations, we expected that laminin ablation from vBM could increase the number of podosome rosettes in blood vessels. To directly test this hypothesis, we stimulated with VEGF-A aortic explants isolated from α_4

laminin subunit null mice[28,29] (*Lama4*−/−). Laminin α_4 is a component of laminin−411, one of the main laminins in vBM (refs 28,29). Genetic ablation of laminin α_4 significantly increased VEGF-A-induced formation of rosettes in ECs of aortic explants (Fig. 4c).

Interestingly, in ECs plated on laminin, the remaining podosome rosettes contained a significantly reduced amount of $\alpha_6\beta_1$ integrin (Supplementary Fig. 6b). Therefore, we evaluated whether the level of $\alpha_6\beta_1$ on the cell surface was modulated by laminin. We observed a pronounced reduction of membrane α_6–GFP, but not of total α_6–GFP, on PMA treatment in the absence of laminin (Fig. 4d and Supplementary Fig. 6c,d). In contrast, when ECs were plated on laminin, the levels of α_6–GFP at the cell surface were not modulated by PMA stimulation (Fig. 4d). Taken together, these results suggest that, when bound to $\alpha_6\beta_1$, laminin blocks this integrin in plasma membrane and, in turn, inhibits rosette formation.

Laminin slows down $\alpha_6\beta_1$ integrin translocation from FAs to podosome rosettes

To further define the relationship between $\alpha_6\beta_1$ integrin dynamics and podosome rosettes, we imaged α_6–GFP and LifeAct–RFP-transduced ECs. During PMA treatment, ECs seeded on laminin formed only classical $\alpha_6\beta_1$-containing FAs (FAs), but not podosome rosettes. In the absence of laminin, $\alpha_6\beta_1$ was instead massively recruited into podosome rosettes that underwent dynamic cycles of continuous assembly and disassembly (Supplementary Video 2). Laminin thus favours the localization of $\alpha_6\beta_1$ into FAs rather than into podosome rosettes (Supplementary Fig. 6e).

To better characterize the reorganization of adhesion sites during rosette formation, we analysed vinculin–RFP-transfected ECs by total internal reflection fluorescence (TIRF) microscopy. Before PMA treatment, vinculin was localized into FAs (Fig. 5a and Supplementary Video 3). After PMA treatment, roughly all FAs disassembled and only a few focal complexes were still visible; then the formation of podosome rosettes became detectable (Fig. 5a and Supplementary Video 3). These results suggest that FA and podosome rosette dynamics are indeed correlated phenomena. Therefore, we studied rosettes in ECs treated with drugs able to modulate FA dynamics. First, we examined whether—as previously suggested[7,9]— the formation of podosome rosettes is independent of direct *de novo* protein synthesis, and we found that the protein-translation inhibitor cycloheximide did not interfere with the induction of rosettes (Fig. 5b). In contrast, the microtubule inhibitor nocodazole completely blocked the appearance of podosome rosettes. As nocodazole stabilizes FA and its ensuing removal results instead in FA disassembly[30], we observed that nocodazole washout, besides favouring FA dismantling, significantly increased the formation of podosome rosettes on PMA treatment. Furthermore, challenging ECs with the recycling inhibitor primaquine extensively impaired the development of podosome rosettes (Fig. 5b) and completely blocked the stimulatory effect of nocodazole washout on rosette formation (Fig. 5b). These results support a model where FA components need to be trafficked to nascent podosome rosettes to allow the formation of the latter (Supplementary Fig. 6f).

The requirement for a PMA-elicited reorganization of ECM adhesions could explain why the binding of laminin to $\alpha_6\beta_1$ integrin, which stabilizes this integrin in FAs, inhibits podosome rosettes. To confirm this hypothesis, we forced FA disassembly in ECs seeded on

laminin. Microtubule-induced FA disassembly was sufficient to rescue the inhibitory effect of laminin on rosette formation (Fig. 5c), not affecting individual podosomes (Supplementary Fig. 6g). Taken together, these results suggest that the level of available $\alpha_6\beta_1$ integrin is a limiting factor for endothelial podosome rosette formation. We therefore analysed rosette incidence in ECs with different levels of $\alpha_6\beta_1$ integrin and seeded on different amounts of laminin. α_6-silenced ECs failed to form rosettes independently of laminin concentration, whereas $\alpha_6\beta_1$-overexpressing ECs showed a high number of rosettes even when seeded on elevated concentrations of laminin (Fig. 5d). Conversely, modulation of $\alpha_6\beta_1$ integrin levels did not affect individual podosomes (Supplementary Fig. 6h). Moreover, the overexpression of α_6 alone was sufficient to promote rosette formation in the absence of VEGF even in cells adhering on laminin (Fig. 5e).

Endothelial podosome rosettes are precursors of new vessel branching points

The presence of endothelial rosettes in the angiogenic endothelium prompted us to investigate their role in sprouting angiogenesis and vessel branching. We studied the formation of podosome rosettes in the mouse aortic ring (mAR) assay[26,31]. This *ex vivo* angiogenesis model is characterized by the formation of VEGF-dependent capillary-like structures producing a vBM sleeve[32] (Supplementary Fig. 7a). Ring-like structures with F-actin/cortactin/MT1-MMP co-localization were detectable in angiogenic sprouts. These ECM-degradative 4-μm-diameter structures were localized in the basal side of ECs (Fig. 6a,b and Supplementary Fig. 7b,c) and are also characterized by localization of integrin α_6 (Supplementary Fig. 7d). Interestingly, the levels of α_6 integrin on the surface of cells containing rosettes, but outside the rosette, were reduced compared with cells without rosettes (Supplementary Fig. 7e,f). This supports the hypothesis of a re-localization of α_6 from the cell surface to endothelial rosettes.

Notably, the localization of podosome rosettes in mAR sprouts was distal from the tip cell (Fig. 6b and Supplementary Video 4), suggesting that these structures were not necessarily involved in tip cell migration, but possibly in the process of branching from pre-existing sprouts. To validate this hypothesis, we performed live-imaging studies on podosome rosettes and lateral vessel branching by exploiting LifeAct-EGFP-expressing transgenic mice[33]. All lateral branches analysed in our study were preceded by the formation of *bona fide* podosome rosettes (Fig. 6c,d and Supplementary Fig. 7f and Supplementary Videos 5 and 6). However, a modest percentage of rosettes (0.5%) effectively produced new sprouts, suggesting that the appearance of rosettes alone is not sufficient to induce lateral branching.

We then analysed mAR branching in the absence of integrin α_6 or laminin. Genetic ablation of endothelial α_6 significantly reduced both the rosette formation (Fig. 3g) and the branching incidence of angiogenic sprouts (Fig. 6e and Supplementary Video 7) without changing the total sprouting length (Supplementary Fig. 7g). Conversely, branching of *Lama4*−/− mARs was significantly enhanced (Fig. 6f and Supplementary Video 8), but the sprout length was not modified (Supplementary Fig. 7h). Moreover, the exogenous addition of laminin rescued the hyper-branched phenotype of *Lama4*−/− mARs (Fig. 6f and Supplementary Video 9).

In vivo blocking of $\alpha_6\beta_1$ integrin impairs endothelial podosome rosette formation and reduces tumour vessel branching

To understand the physio-pathological relevance of endothelial podosome rosettes in the angiogenic process, we treated RipTag2 mice with the anti-α_6 blocking antibody. We first tested the accessibility of anti-α_6 to endothelial podosome rosettes[26,34]. Ten minutes after injection in RipTag2 mice, the anti-α_6 antibody was sharply localized in podosome rosettes of tumour blood vessels (Fig. 7a and Supplementary Fig. 7i).

To evaluate the effects of anti-α_6 on endothelial rosettes, we treated RipTag2 mice for 2 weeks by starting antibody administration at the beginning of the angiogenic stage. The blockade of $\alpha_6\beta_1$ integrin caused a strong reduction of podosome rosette density (Fig. 7a) and concomitantly a decrease of vessel branching (Fig. 7c).

To confirm the results obtained with anti-α_6 treatment, we analysed rosette density in vessels of B16F10 xenograft and ischaemic tissues from endothelial α_6 integrin null mice. Genetic endothelial ablation of α_6 integrin effectively impaired podosome rosettes in both models (Fig. 7d,e). B16F10 tumours showed that α_6 integrin ablation significantly reduced blood vessel branching in tumours (Fig. 7f), confirming our ex vivo results (Fig. 6e). Notably, integrin α_6 localized to podosome rosettes also in angiogenic vessels of human lung tumours (Supplementary Fig. 7l).

DISCUSSION

In the adult organism, blood vessels are usually quiescent and rarely form new branches. ECs and mural cells share a vBM that forms a sleeve around endothelial tubules and prevents resident ECs from leaving their positions[4,35,36]. However, ECs are able to promptly respond to angiogenic signals. The mechanisms controlling vBM proteolytic breakdown and selection of the ECs that steer lateral branches are still poorly understood. Here, we show that angiogenic endothelium forms subcellular structures with degradative activity, called podosome rosettes, which precede the emergence of new lateral sprouts.

It is known that MMPs—including MT1-MMP—correlate with angiogenesis, by letting ECs breach the vBM and enter tissues[6,37]. Spatial and temporal control of these proteinases is essential for an efficient sprouting. In angiogenic ECs podosome rosettes are plasma membrane regions where MT1-MMP is enriched. Indeed, it is reasonable that constrained degradation of vBM is preferable to diffuse and uncontrolled proteinase activity.

Furthermore, podosome rosettes are also adhesive structures containing integrins. Notably, in a model of BM invasion in *Caenorhabditis elegans*[38], the integrin heterodimer INA-1/PAT-3— highly homologous with mammalian $\alpha_6\beta_1$—is crucial for cell invasion through BM (ref. 38). Here we show that the assembly of podosome rosettes in ECs depends on $\alpha_6\beta_1$ as well, thus supporting the idea that endothelial podosome rosettes are specialized structures for vBM invasion in vertebrates.

Whereas endothelial podosome rosettes are involved in the sprouting process of vessels embedded in a thick vBM, such as adult vessels, they do not play a relevant role when vBM

is absent, such as during early vascular development[39,40]. This might explain why loss of integrin α_6, laminin α_4 or MT1-MMP does not impair vascular development in embryos, but affects pathological angiogenesis in mature tissues[6,19,29].

Importantly, we demonstrated that VEGF-A stimulation induces the assembly of endothelial rosettes, but does not reduce the individual podosomes. This effect largely depends on $\alpha_6\beta_1$ integrin, which is transcriptionally induced by VEGF-A. Recent evidence shows that both FAK and β_1 integrin are required for podosome rosette assembly and stabilization[13,24]. However, the molecular mechanisms leading to the formation of podosome rosettes remain elusive. Here, we show that $\alpha_6\beta_1$ contributes to the stability of podosome rosettes and that high levels of $\alpha_6\beta_1$ are needed within podosome rosettes to increase their lifespans (Fig. 3e).

The transition from a quiescent to a migratory cellular phenotype is often characterized by FA disassembly followed by the formation of invadopodia or podosomes[16,23,41]. Our data, showing that both disassembly of FAs and recycling of their components are necessary for rosette formation, unveil a direct link between FAs and rosettes (Supplementary Fig. 6f). In this context, laminin of vBM hampers rosette formation by sequestering $\alpha_6\beta_1$ in FAs. The upregulation of α_6—induced by angiogenic growth factor stimulation—could overcome the anti-angiogenic effect of vBM by increasing the $\alpha_6\beta_1$ available for the formation of podosome rosettes, which in turn will allow vBM cleavage and angiogenesis.

The molecular actors that modulate adult vasculature geometry are poorly defined. The tortuosity and high branching index of tumour vasculature often make it ‘non-functional’, characterized by an impaired blood supply[42] and interstitial hypertension[43], which compromise drug delivery[44]. Notably, all angiogenic vessels that we analysed exhibited podosome rosettes but we could not detect them in quiescent vessels. This specific distribution suggests that endothelial podosome rosettes are determinants of angiogenic vessels. Indeed, we showed that inhibition of podosome rosette formation by $\alpha_6\beta_1$ blockade or genetic deletion affects vessel branching (Fig. 6e and Fig. 7c,f). Consistently, previous evidence showed how inhibition or genetic ablation of $\alpha_6\beta_1$ integrin in ECs impaired tumoral and post-ischaemic angiogenesis[19,26]. In contrast, genetic ablation of laminin α_4—described to give hyper-branched angiogenesis in the adult animal—promotes rosette formation and enhances endothelial sprouting[29,45]. The control exerted by $\alpha_6\beta_1$ integrin on tumour blood vessel branching as a consequence of podosome rosette inhibition in ECs supports the previously proposed notion of vascular normalization by suggesting endothelial podosome rosettes as a new target to normalize tumour vasculature.

In summary, this work describes the role of endothelial podosome rosettes as precursors of sprouting angiogenesis and important determinants of the vascular branching in tumour angiogenesis. We proposed a model (Fig. 7g) where quiescent vessels are characterized by low levels of $\alpha_6\beta_1$ integrin, recruited in FAs and bound to the vBM laminin. This hampers the formation of podosome rosettes, reducing the sprouting ability. When a tumour persistently produces VEGF, α_6 integrin is upregulated in ECs. The increased availability of $\alpha_6\beta_1$ integrin allows the formation and stabilization of endothelial podosome rosettes and the ensuing MMP-driven modulation of ECM that, in turn, leads vBM invasion by ECs and sprouting angiogenesis.

METHODS

Methods and any associated references are available in the online version of the paper.

Supplementary Material

Refer to Web version on PubMed Central for supplementary material.

ACKNOWLEDGEMENTS

A special thank you to E. Georges-Labouesse (CNRS/INSERM/ULP, Illkirch, France), who recently passed away, for kindly providing Tie2-dependent integrin α_6 KO mice. We thank P. C. Marchisio (San Raffaele Scientific Institute, Milano, Italy) for discussion and insightful suggestions on the manuscript; D. R. Sherwood (Duke University Medical Center, Durham, USA) for critical reading of the manuscript; K. Tryggvason (Karolinska Institutet, Stockholm, Sweden) for providing laminin α_4 null mice; R. Wedlich-Söldner (Max-Planck Institute of Biochemistry, Martinsried, Germany) and L. M. Machesky (Beatson Institute for Cancer Research, Glasgow, UK) for providing breeding pairs for the LifeAct-EGFP mouse colony and reagents; R. Falcioni (National Cancer Institute 'Regina Elena', Rome, Italy) for critical reading and reagents; E. De Luca and M. Gai (MBC, Torino, Italy) for their assistance in multiphoton microscopy; Y. Boucher and C. Smith (HMS, Boston, USA) for assistance in immunohistochemistry on human tissues; and E. Giraudo and F Maione (IRCC, Candiolo, Italy) for their help in the treatment of RipTag2 mice. This work was supported by Associazione Italiana per la Ricerca sul Cancro (AIRC) investigator grants IG (10133, F.B.; 14635, L.P; 13016 G Serini) and fellowships (13604 G Seano; 15026 P.A.G.); AIRC 5×1000 (12182); Converging Technologies Program, grant: 'Photonic Biosensors for Early Cancer Diagnostics'; Technological Platforms for Biotechnology: grant DRUIDI; Fondazione Cassa di Risparmio Torino (CRT); Fondazione Piemontese per la Ricerca sul Cancro-ONLUS (Intramural Grant 5×1000 2008) (L.P); Fondo Investimenti per la Ricerca di Base RBAP11BYNP (Newton) (FB. and L.P); University of Torino-Compagnia di San Paolo: RETHE grant (F.B.); GeneRNet grant (L.P); P01 CA080124/CA/NCI NIH HHS/United States (R.K.J.); The 'Fondazione T & L. de Beaumont Bonelli' and the Girardi Family (G Seano).

References

1. Hallmann R, et al. Expression and function of laminins in the embryonic and mature vasculature. Physiol. Rev. 2005; 85:979–1000. [PubMed: 15987800]
2. Ferrara N, Gerber HP, LeCouter J. The biology of VEGF and its receptors. Nat. Med. 2003; 9:669–676. [PubMed: 12778165]
3. Inoue M, Hager JH, Ferrara N, Gerber HP, Hanahan D. VEGF-A has a critical, nonredundant role in angiogenic switching and pancreatic beta cell carcinogenesis. Cancer Cell. 2002; 1:193–202. [PubMed: 12086877]
4. Carmeliet P, Jain RK. Molecular mechanisms and clinical applications of angiogenesis. Nature. 2011; 473:298–307. [PubMed: 21593862]
5. Galvez BG, Matias-Roman S, Albar JP, Sanchez-Madrid F, Arroyo AG. Membrane type 1-matrix metalloproteinase is activated during migration of human endothelial cells and modulates endothelial motility and matrix remodeling. J. Biol. Chem. 2001; 276:37491–37500. [PubMed: 11448964]
6. Yana I, et al. Crosstalk between neovessels and mural cells directs the site-specific expression of MT1-MMP to endothelial tip cells. J. Cell Sci. 2007; 120:1607–1614. [PubMed: 17405818]
7. Linder S, Aepfelbacher M. Podosomes: adhesion hot-spots of invasive cells. Trends Cell Biol. 2003; 13:376–385. [PubMed: 12837608]
8. Gimona M, Buccione R, Courtneidge SA, Linder S. Assembly and biological role of podosomes and invadopodia. Curr. Opin. Cell Biol. 2008; 20:235–241. [PubMed: 18337078]
9. Tarone G, Cirillo D, Giancotti FG, Comoglio PM, Marchisio PC. Rous sarcoma virus-transformed fibroblasts adhere primarily at discrete protrusions of the ventral membrane called podosomes. Exp. Cell Res. 1985; 159:141–157. [PubMed: 2411576]
10. Mizutani K, Miki H, He H, Maruta H, Takenawa T. Essential role of neural Wiskott-Aldrich syndrome protein in podosome formation and degradation of extracellular matrix in src-transformed fibroblasts. Cancer Res. 2002; 62:669–674. [PubMed: 11830518]

11. Rottiers P, et al. TGFβ-induced endothelial podosomes mediate basement membrane collagen degradation in arterial vessels. J. Cell Sci. 2009; 122:4311–4318. [PubMed: 19887587]
12. Varon C, et al. Transforming growth factor beta induces rosettes of podosomes in primary aortic endothelial cells. Mol. Cell. Biol. 2006; 26:3582–3594. [PubMed: 16611998]
13. Pan YR, Chen CL, Chen HC. FAK is required for the assembly of podosome rosettes. J. Cell Biol. 2011; 195:113–129. [PubMed: 21969470]
14. Riedl J, et al. Lifeact: a versatile marker to visualize F-actin. Nat. Methods. 2008; 5:605–607. [PubMed: 18536722]
15. Buccione R, Orth JD, McNiven MA. Foot and mouth: podosomes, invadopodia and circular dorsal ruffles. Nat. Rev. Mol. Cell Biol. 2004; 5:647–657. [PubMed: 15366708]
16. Murphy DA, Courtneidge SA. The 'ins' and 'outs' of podosomes and invadopodia: characteristics, formation and function. Nat. Rev. Mol. Cell Biol. 2011; 12:413–426. [PubMed: 21697900]
17. Prewett M, et al. Antivascular endothelial growth factor receptor (fetal liver kinase 1) monoclonal antibody inhibits tumor angiogenesis and growth of several mouse and human tumors. Cancer Res. 1999; 59:5209–5218. [PubMed: 10537299]
18. Couffinhal T, et al. Mouse model of angiogenesis. Am. J. Pathol. 1998; 152:1667–1679. [PubMed: 9626071]
19. Bouvard C, et al. Tie2-dependent knockout of α6 integrin subunit in mice reduces post-ischaemic angiogenesis. Cardiovasc. Res. 2012; 95:39–47. [PubMed: 22517984]
20. Herbst RS, Onn A, Sandler A. Angiogenesis and lung cancer: prognostic and therapeutic implications. J. Clin. Oncol. 2005; 23:3243–3256. [PubMed: 15886312]
21. Hadler-Olsen E, et al. Gelatin *in situ* zymography on fixed, paraffin-embedded tissue: zinc and ethanol fixation preserve enzyme activity. J. Histochem. Cytochem. 2010; 58:29–39. [PubMed: 19755718]
22. Hanahan D. Heritable formation of pancreatic β-cell tumours in transgenic mice expressing recombinant insulin/simian virus 40 oncogenes. Nature. 1985; 315:115–122. [PubMed: 2986015]
23. Block MR, et al. Podosome-type adhesions and focal adhesions, so alike yet so different. Eur. J. Cell Biol. 2008; 87:491–506. [PubMed: 18417250]
24. Destaing O, et al. β1A integrin is a master regulator of invadosome organization and function. Mol. Biol. Cell. 2010; 21:4108–4119. [PubMed: 20926684]
25. Schmidt S, et al. Kindlin-3-mediated signaling from multiple integrin classes is required for osteoclast-mediated bone resorption. J. Cell Biol. 2011; 192:883–897. [PubMed: 21357746]
26. Primo L, et al. Increased expression of α6 integrin in endothelial cells unveils a proangiogenic role for basement membrane. Cancer Res. 2010; 70:5759–5769. [PubMed: 20570893]
27. Lee TH, et al. Integrin regulation by vascular endothelial growth factor in human brain microvascular endothelial cells: role of $\alpha_6\beta_1$ integrin in angiogenesis. J. Biol. Chem. 2006; 281:40450–40460. [PubMed: 17085437]
28. Thyboll J, et al. Deletion of the laminin α4 chain leads to impaired microvessel maturation. Mol. Cell Biol. 2002; 22:1194–1202. [PubMed: 11809810]
29. Zhou Z, et al. Deletion of laminin-8 results in increased tumor neovascularization and metastasis in mice. Cancer Res. 2004; 64:4059–4063. [PubMed: 15205311]
30. Ezratty EJ, Partridge MA, Gundersen GG. Microtubule-induced focal adhesion disassembly is mediated by dynamin and focal adhesion kinase. Nat. Cell Biol. 2005; 7:581–590. [PubMed: 15895076]
31. Seano G, et al. Modeling human tumor angiogenesis in a three-dimensional culture system. Blood. 2013; 121:e129–e137. [PubMed: 23471306]
32. Schmidt M, et al. EGFL7 regulates the collective migration of endothelial cells by restricting their spatial distribution. Development. 2007; 134:2913–2923. [PubMed: 17626061]
33. Riedl J, et al. Lifeact mice for studying F-actin dynamics. Nat. Methods. 2010; 7:168–169. [PubMed: 20195247]
34. Magnussen A, et al. Rapid access of antibodies to $\alpha_5\beta_1$ integrin overexpressed on the luminal surface of tumor blood vessels. Cancer Res. 2005; 65:2712–2721. [PubMed: 15805270]

35. Eble JA, Niland S. The extracellular matrix of blood vessels. Curr. Pharm. Des. 2009; 15:1385–1400. [PubMed: 19355976]

36. Yousif LF, Di Russo J, Sorokin L. Laminin isoforms in endothelial and perivascular basement membranes. Cell Adhes. Migr. 2013; 7:101–110.

37. De Smet F, Segura I, De Bock K, Hohensinner PJ, Carmeliet P. Mechanisms of vessel branching: filopodia on endothelial tip cells lead the way. Arterioscler. Thromb. Vasc. Biol. 2009; 29:639–649. [PubMed: 19265031]

38. Hagedorn EJ, et al. Integrin acts upstream of netrin signaling to regulate formation of the anchor cell's invasive membrane in C. elegans. Dev. Cell. 2009; 17:187–198. [PubMed: 19686680]

39. Iivanainen A, et al. Primary structure, developmental expression, and immunolocalization of the murine laminin α4 chain. J. Biol. Chem. 1997; 272:27862–27868. [PubMed: 9346933]

40. Patton BL, Miner JH, Chiu AY, Sanes JR. Distribution and function of laminins in the neuromuscular system of developing, adult, and mutant mice. J. Cell Biol. 1997; 139:1507–1521. [PubMed: 9396756]

41. Chan KT, Cortesio CL, Huttenlocher A. FAK alters invadopodia and focal adhesion composition and dynamics to regulate breast cancer invasion. J. Cell Biol. 2009; 185:357–370. [PubMed: 19364917]

42. Mazzone M, et al. Heterozygous deficiency of PHD2 restores tumor oxygenation and inhibits metastasis via endothelial normalization. Cell. 2009; 136:839–851. [PubMed: 19217150]

43. Jain RK. Normalizing tumor microenvironment to treat cancer: bench to bedside to biomarkers. J. Clin. Oncol. 2013; 31:2205–2218. [PubMed: 23669226]

44. Jain RK. Normalization of tumor vasculature: an emerging concept in antiangiogenic therapy. Science. 2005; 307:58–62. [PubMed: 15637262]

45. Stenzel D, et al. Endothelial basement membrane limits tip cell formation by inducing Dll4/Notch signalling in vivo. EMBO Rep. 2011; 12:1135–1143. [PubMed: 21979816]

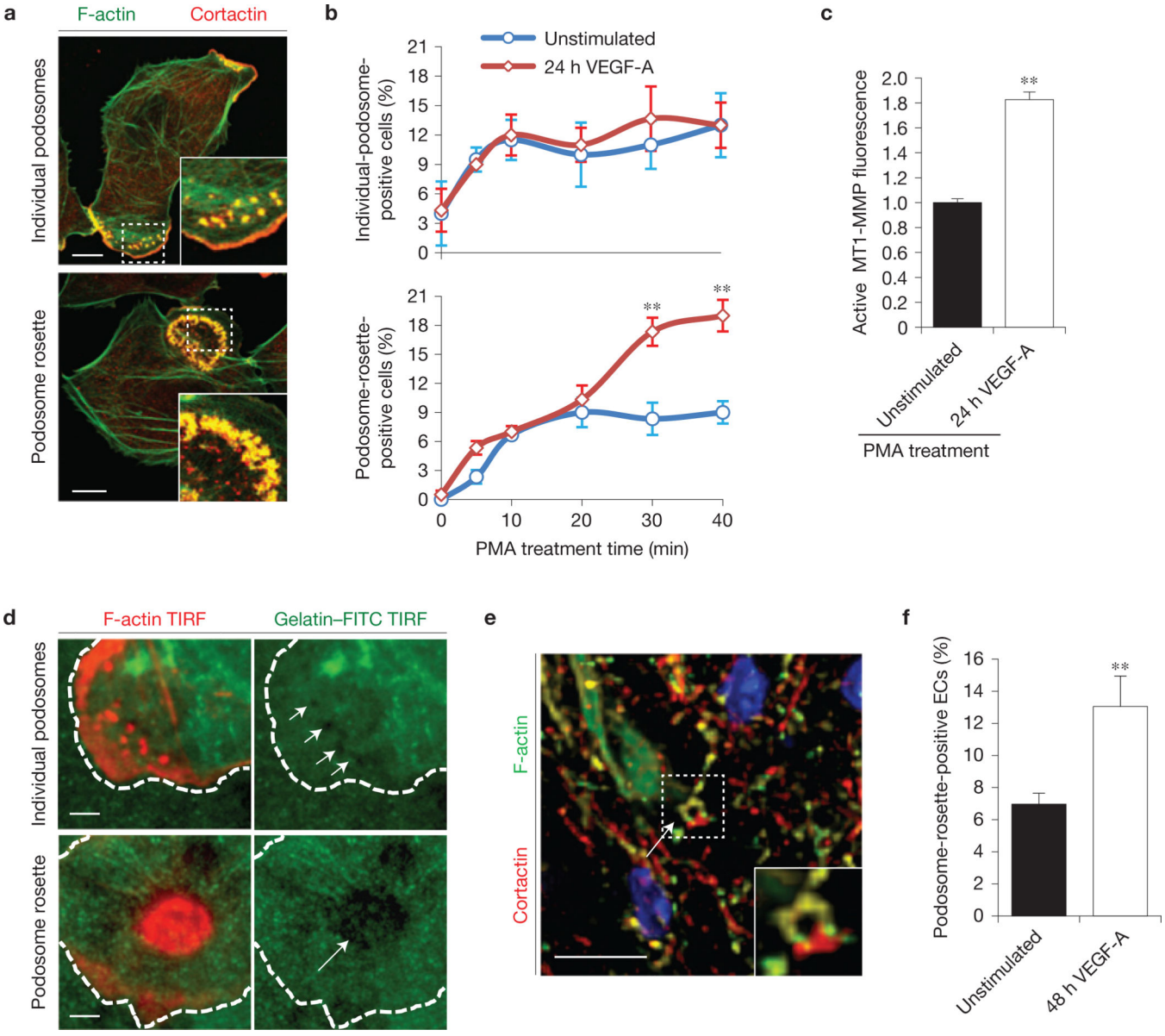

Figure 1.

VEGF-A induces endothelial podosome rosettes. (**a**) Immunostained representative ECs treated with PMA for 30 min. Insets, zoom of the same micrograph. Scale bars, 10 μm. (**b**) ECs—incubated for 24 h in M199 10% FCS (unstimulated) or in M199 10% FCS plus 30 ng ml^{-1} of VEGF-A (24 h VEGF-A)—were treated for 30 min with PMA. We calculated the percentage of individual-podosome- and podosome-rosette-positive ECs, treated with PMA for the indicated times. Mean ± s.e.m. of $n = 3$ independent experiments in which 250 cells were analysed per experimental point. (**c**) Cytofluorimetric analysis of the active form of MT1-MMP. ECs treated with PMA for 30 min. Normalized mean ± s.e.m. of $n = 3$ independent experiments in which 9×10^4 cells were analysed per experimental point. (**d**) Gelatin degradation assay by TIRF micrographs. ECs were seeded on FITC-conjugated gelatin, PMA-treated and then stained with phalloidin. The white dashed line is the outline

of the cell boundary and is traced here as a guide to the eye. White arrows indicate the areas in which gelatin was degraded by individual podosomes or podosome rosettes. Scale bars, 10 μm. (**e,f**) *Ex vivo* VEGF-A stimulation induces podosome rosettes in aortic vessels. Aortic explants were incubated for 48 h in M199 10% FCS (unstimulated) or M199 10% FCS with 30 ng ml^{-1} of VEGF-A (48 h VEGF-A). (**e**) Immunostaining of a representative 48 h VEGF-A-stimulated aortic explant. Inset, a podosome rosette. Scale bar, 20 μm. Single-channel images are in Supplementary Fig. 1e. (**f**) Graph showing the percentage of podosome-rosette-positive ECs in the endothelial layer of aortic explants. Mean ± s.e.m. of n=3 independent experiments in which 511 nuclei were analysed per experimental point. (**b,c,f**) Statistical significance was calculated using an unpaired non-parametric Mann-Whitney test (**P<0.01 versus unstimulated.).

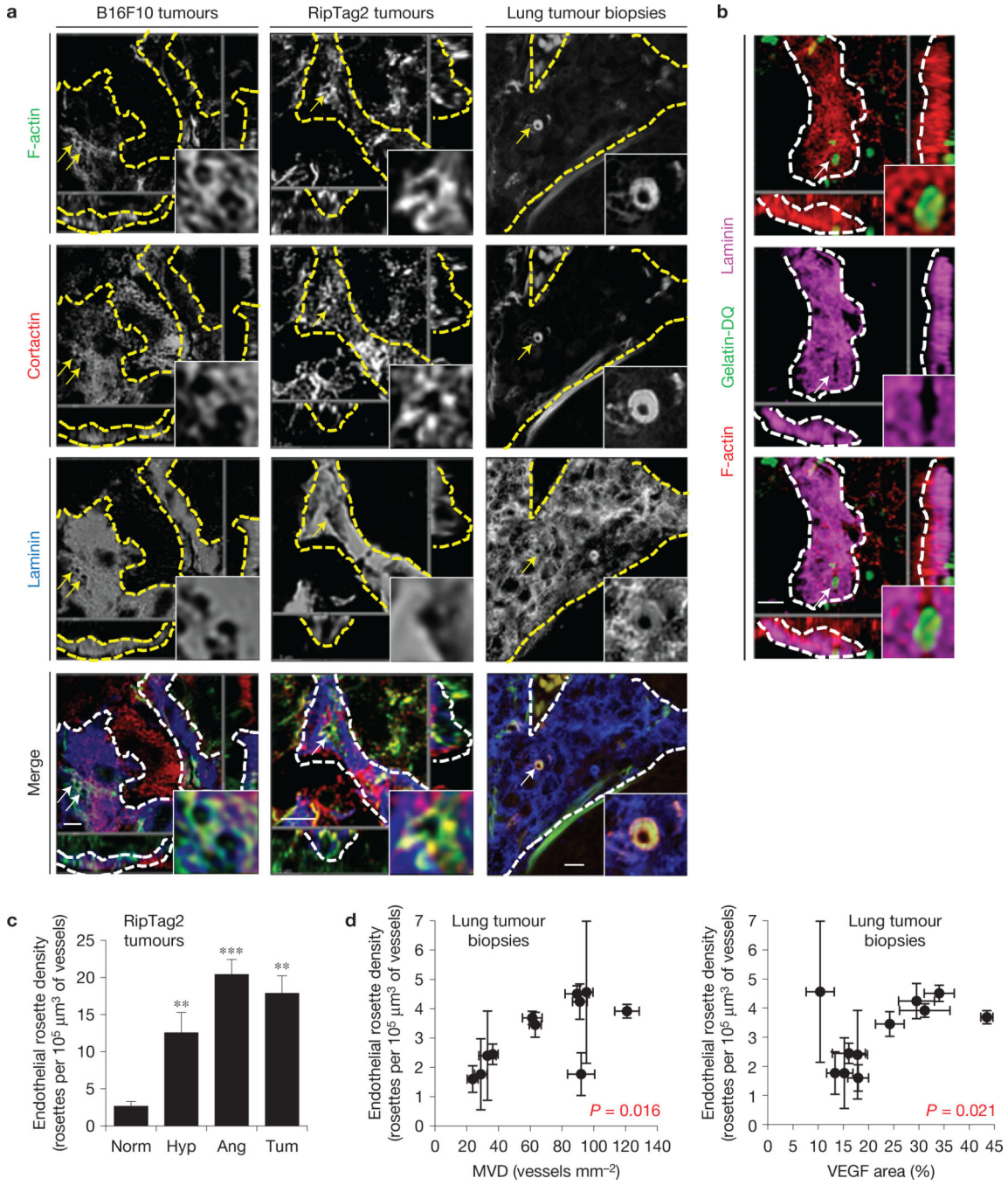

Figure 2.

Tumour angiogenic vessels are characterized by high levels of endothelial podosome rosettes. (**a**) Confocal imaging stacks of representative vessels in subcutaneous B16F10 melanoma, in angiogenic islets of transgenic RipTag2 mice or human samples of lung tumours. *xyz*-section of immunostaining for primary antibodies as indicated. Vessels are delimited by dashed lines; arrows indicate podosome rosettes. Inset, the podosome rosette. Schematization and 3D rendering in Supplementary Fig. 2a,b. Scale bars, 10 µm. (**b**) *In situ* zymography in RipTag2 angiogenic islets. *xyz*-section of staining for primary antibodies as

indicated and gelatin-DQ (dye-quenched), showing the degradated gelatin. Vessels are delimited by white dashed lines; white arrows indicate podosome rosettes. Inset, the podosome rosette. 3D rendering in Supplementary Fig. 2e. Scale bar, 10μm. (**c**) Graph shows the density of podosome rosettes in vessels of RipTag2 tumour mouse stages. Vessel regions of interest were determined with laminin staining. Mean ± s.e.m. of $n = 3$ mice, 5 fields per tumour stage. Statistical significance was calculated using a one-way ANOVA test followed by Bonferroni-adjusted *post hoc t*-tests (**$P<0.01$ versus normal islets; ***$P < 0.001$ versus normal islets). (**d**) Scatter plots of the density of endothelial podosome rosettes versus microvessel density (MVD)-CD31 ($r^2=0.49$, $P = 0.016$) and VEGF area fraction in biopsy samples of lung tumours ($r^2=0.46$, $P = 0.021$). Mean ± s.e.m. of $n = 3$ different vessels per biopsy for rosette density and $n = 20$ fields per slide for MVD and VEGF. Statistical significance was calculated using a Pearson correlation test. Representative images are shown in Supplementary Fig. 3c.

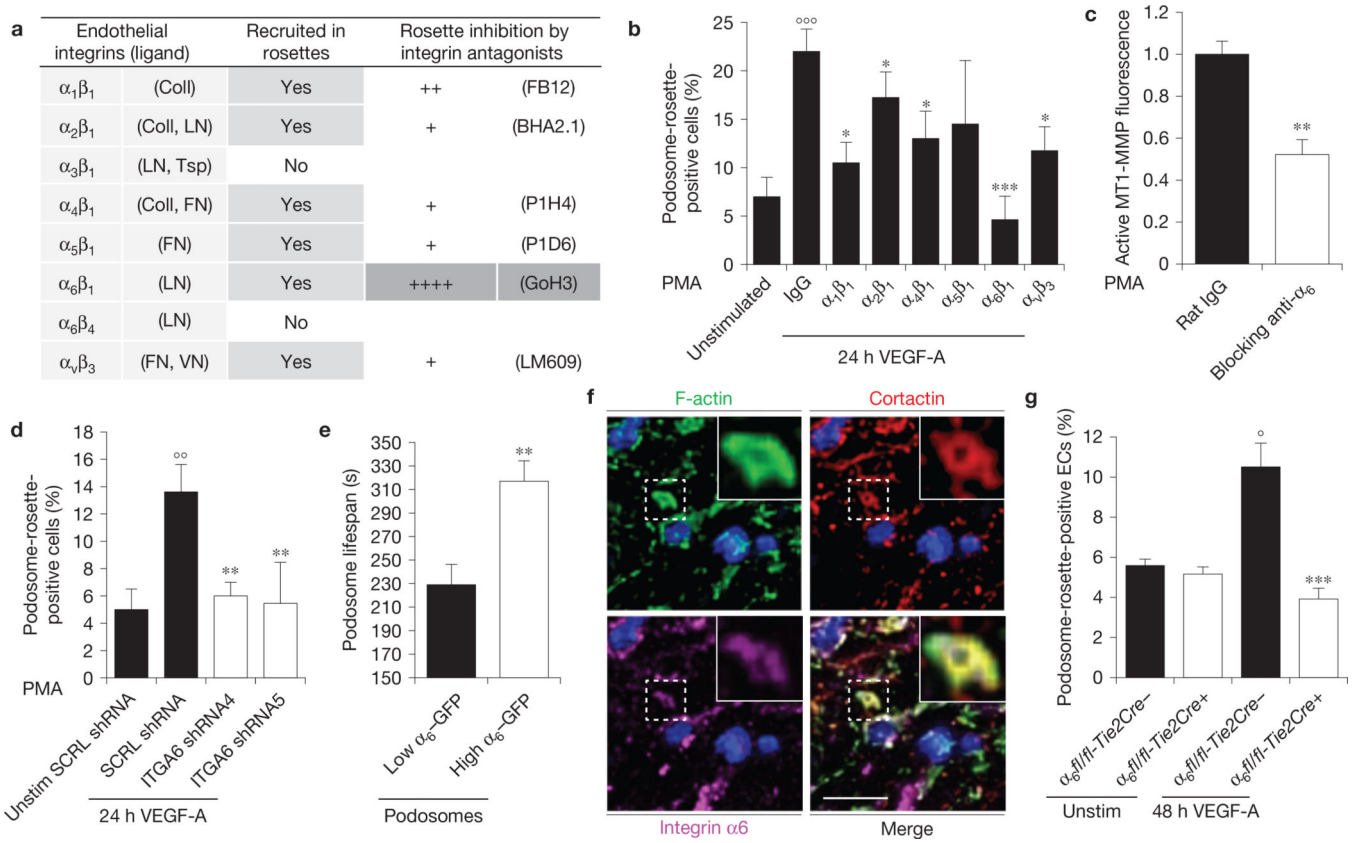

Figure 3.

Integrin α_6 is essential for VEGF-induced endothelial podosome rosette formation and function. (**a**) Table of integrin recruitment in endothelial podosome rosettes and functional blocking treatment. The qualitative analysis of rosette blockade is based on podosome-rosette-positive cells percentages in comparison with aspecific IgG treatment. Confocal micrographs of integrin recruitment are shown in Supplementary Fig. 4a. (**b**) Graph showing the percentages of podosome-rosette-positive ECs, stimulated as indicated and treated with aspecific IgG or anti-integrin blocking antibodies 2 h before PMA treatment. ECs were treated with IgG or anti-integrin blocking antibody (20 μg ml^{-1}) during cell adhesion and then stimulated with PMA for 30 min. Mean ± s.e.m. of $n = 3$ independent experiments in which 250 cells were analysed per experimental point. Statistical significance was calculated using a one-way ANOVA test followed by Bonferroni-adjusted *post hoc t*-tests (°°°$P<0.001$ versus unstimulated; *$P<0.05$ versus 24 h VEGF-A IgG; ***$P<0.001$ versus 24 h VEGF-A IgG). (**c**) Cytofluorimetric analysis of active MT1-MMP in VEGF-A-stimulated ECs, treated with rat IgG or anti-α_6 blocking antibody and then stimulated with PMA for 30 min. Normalized mean ± s.e.m. of $n = 3$ independent experiments in which 9×10^4 cells were analysed per experimental point. Statistical significance was calculated using an unpaired non-parametric Mann-Whitney test (**$P<0.01$ versus rat IgG). (**d**) Graph showing the percentages of podosome-rosette-positive ECs, transduced with scramble (SCRL) shRNA or shRNA against integrin α_6 (ITGA6 shRNA4 and ITGA6 shRNA5). Membrane integrin α_6 levels in transduced ECs are shown in Supplementary Fig. 4d. Mean ± s.e.m. of $n = 3$ independent experiments in which 250 cells were analysed per experimental point.

Statistical significance was calculated using a one-way ANOVA test followed by Bonferroni-adjusted *post hoc t*-tests (°°P<0.01 versus Unstim SCRL shRNA; **P<0.01 versus SCRL shRNA). (**e**) Lifespan of the podosomes that form endothelial rosettes in α_6-GFP- and LifeAct-RFP-transduced ECs. Graph shows the lifespan in minutes of podosomes with low or high levels of integrin α_6 detected with TIRF microscopy (90 nm of depth) in VEGF-stimulated ECs. Mean ± s.e.m. of n = 230 podosomes from 3 different cells. Statistical significance was calculated using an unpaired non-parametric Mann-Whitney test (**P< 0.01 versus low ITGA6). (**f**) Endothelial layer of a 48 h VEGF-A-stimulated aortic explant immunostained by the indicated antibodies and nuclear-stained by DAPI (blue). Inset, a podosome rosette in the basal side of the endothelial layer. Scale bar, 20 μm. (**g**) VEGF-A stimulation in aortic explants of Tie2-dependent α_6 null mice. Aortic explants from WT (α_6*fl/fl-Tie2Cre*−) or endothelial α_6 null (α_6*fl/fl-Tie2Cre*+) mice were incubated for 48 h in M199 10% FCS (unstim) or M199 10% FCS with 30 ng ml^{-1} of VEGF-A (48 h VEGF-A). Mean ± s.e.m. of n = 3 independent experiments in which 1,250 nuclei were analysed per experimental point. Statistical significance was calculated using two-way ANOVA test followed by Bonferroni-adjusted *post hoc t*-tests (°P<0.05 versus unstim α_6*fl/fl-Tie2Cre*−; ***P<0.001 versus 48 h VEGF-A α_6*fl/fl-Tie2Cre*−).

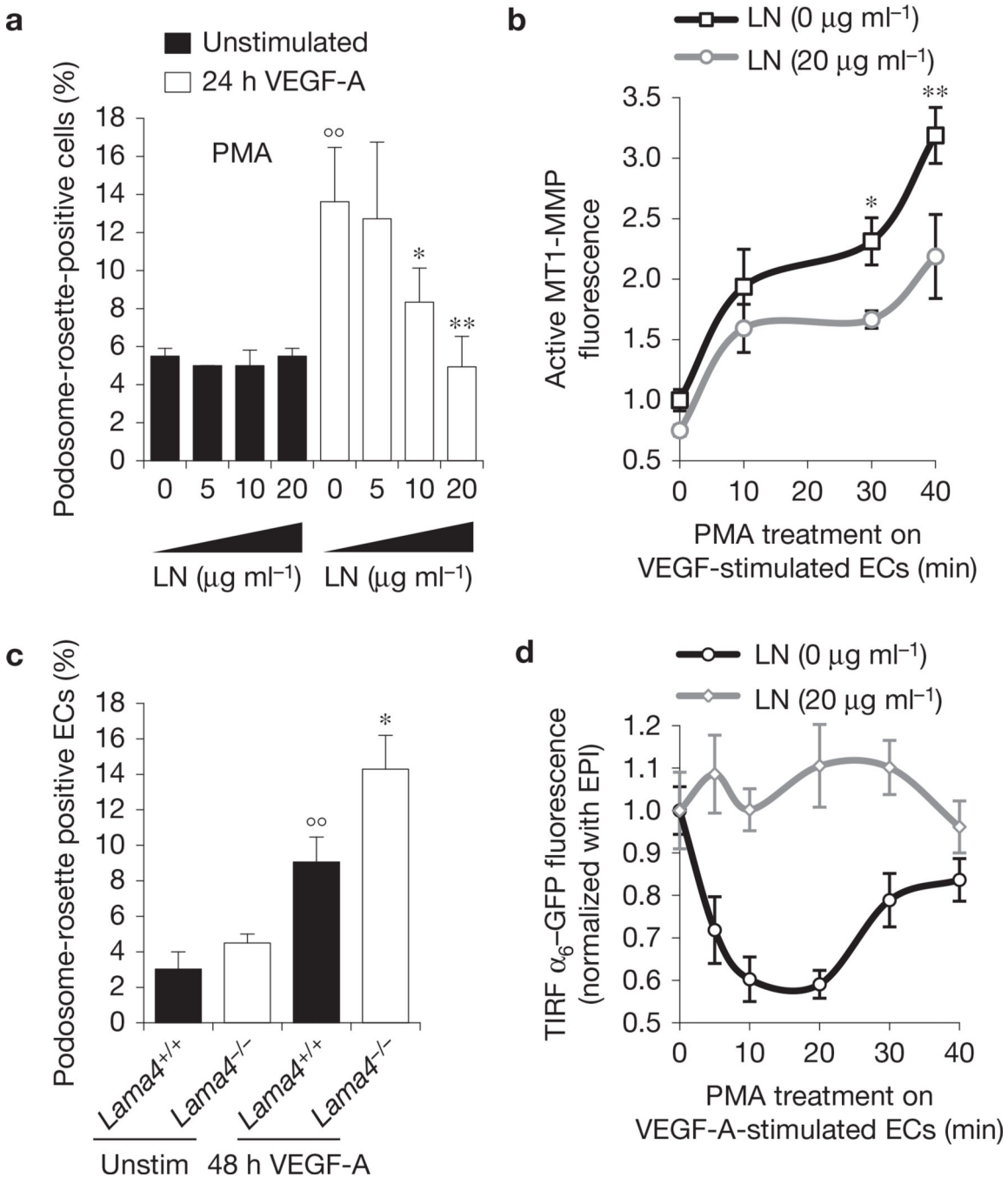

Figure 4.

Laminin impairs podosome rosette formation. (**a**) Graph showing the percentages of podosome-rosette-positive ECs, stimulated as indicated, seeded on gelatin-coated coverslips with the indicated addition of laminin. Percentages of individual-podosome-positive cells are in Supplementary Fig. 6a. Mean ± s.e.m. of $n = 3$ independent experiments in which 260 cells were analysed per experimental point. Statistical significance was calculated using a two-way ANOVA test followed by Bonferroni-adjusted *post hoc t*-tests (°° $P<0.01$ versus unstimulated; *$P<0.05$ versus LN (0 μg ml $^{-1}$); **$P<0.01$ versus LN (0 μg ml^{-1})). (**b**)

Cytofluorimetric analysis of active MT1-MMP in VEGF-stimulated ECs, seeded on a gelatin coating with the indicated addition of laminin. Normalized mean ± s.e.m. of $n = 3$ independent experiments in which 10^5 cells were analysed per experimental point. Statistical significance was calculated using a two-way ANOVA test followed by Bonferroni-adjusted *post hoc t*-tests (**P*<0.05 versus LN (0 μg ml^{-1}); ***P* < 0.01 versus LN (0 g ml^{-1})). (**c**) VEGF-A stimulation in aortic explants of laminin α_4 null mice. Aortic explants from *Lama4*$^{+/+}$ or *Lama4*−/− mice were incubated for 48 h in M199 10% FCS (unstim) or M199 10% FCS with 30 ng ml^{-1} of VEGF-A (48 h VEGF-A). Mean ± s.e.m. of $n = 3$ independent experiments in which 550 nuclei were analysed per experimental point. Statistical significance was calculated using a two-way ANOVA test followed by Bonferroni-adjusted *post hoc t*-tests (°° *P* < 0.05 versus unstimulated *Lama4*$^{+/+}$; **P*<0.05 versus 48 h VEGF-A *Lama4*$^{+/+}$). (**d**) Integrin α_6 membrane localization is modulated by laminin in the substratum. The graph shows the ratio of α_6-GFP fluorescence in the membrane (TIRF microscopy with <90 nm of deepness) and in the whole cell (epifluorescence, EPI) in the indicated periods of PMA treatment; mean ± s.e.m. of $n = 30$ cells from 3 independent experiments.

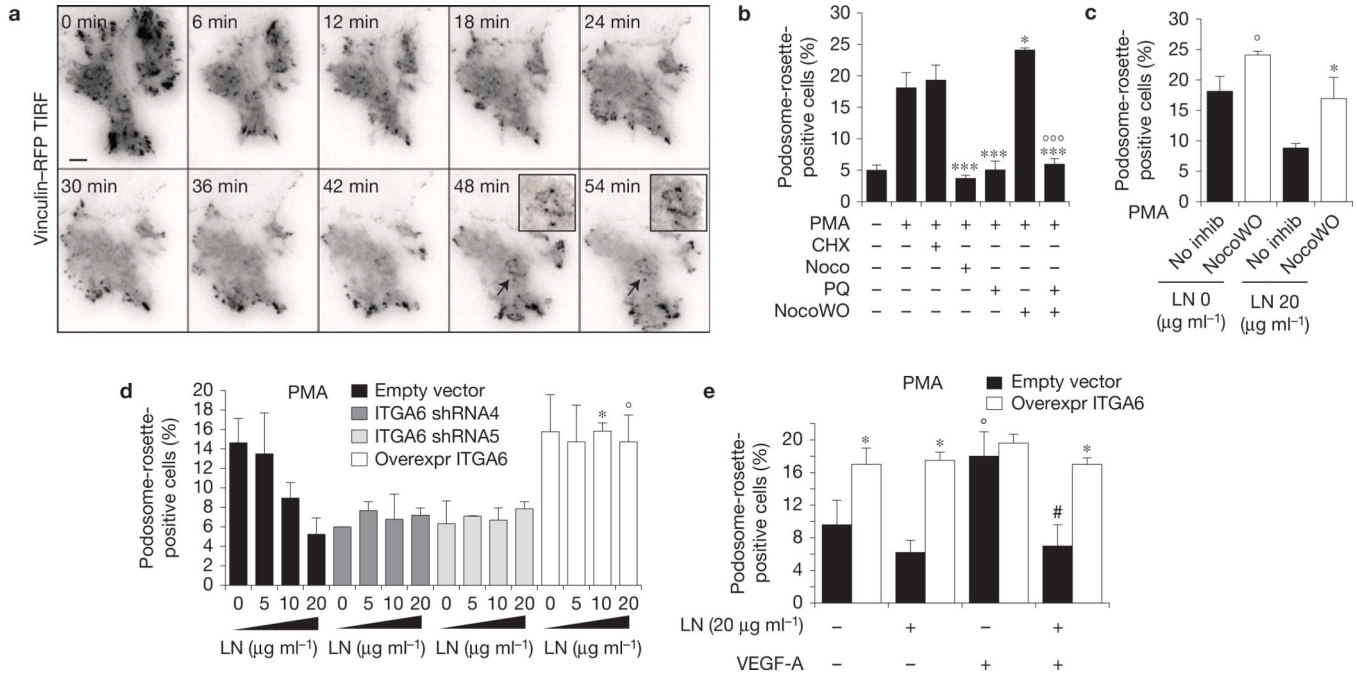

Figure 5.

α_6 integrin–laminin binding in FAs slows down α_6 integrin translocation to podosome rosettes. (**a**) Time-lapse TIRF microscopy of vinculin–RFP-transfected ECs during PMA treatment. Insets, podosome rosettes indicated by arrows. For complete video, see Supplementary Video 3. Scale bar, 20 μm. (**b**) Graph showing the percentages of podosome-rosette-positive ECs, treated as indicated. CHX: cycloheximide; Noco: nocodazole; PQ: primaquine; NocoWO: nocodazole washout. Mean ± s.e.m. of $n = 3$ independent experiments in which 200 cells were analysed per experimental point. Statistical significance was calculated using a one-way ANOVA test followed by Bonferroni-adjusted *post hoc t*-tests ***P<0.05 versus PMA treated; ***P< 0.001 versus PMA treated; °°°P< 0.001 versus NocoWO+PMA). (**c**) Graph showing the percentages of podosome-rosette-positive ECs, seeded on gelatin-coated coverslips with the indicated laminin addition and PMA-stimulated with or without nocodazole washout. Percentages of individual-podosome-positive cells are in Supplementary Fig. 6g. Mean ± s.e.m. of n=3 independent experiments in which 230 cells were analysed per experimental point. Statistical significance was calculated using a two-way ANOVA test followed by Bonferroni-adjusted *post hoc t*-tests (°P<0.05 versus no inhib LN (0 μg ml^{-1}); *P< 0.05 versus no inhib LN (20 μg ml^{-1})). (**d**) Graph showing the percentages of podosome-rosette-positive ECs, seeded on gelatin-coated coverslips with the indicated addition of laminin. ECs were transduced as indicated. Membrane integrin α_6 levels in transduced ECs are shown in Supplementary Fig. 4d. Percentages of individual-podosome-positive cells are in Supplementary Fig. 6h. Mean ± s.e.m. of n= 3 independent experiments in which 320 cells were analysed per experimental point. Statistical significance was calculated using one-way ANOVA test followed by Bonferroni-adjusted *post hoc t*-tests (*P<0.05 versus empty vector L(10 μg ml^{-1}); °P < 0.05 versus empty vector L(20 μg ml^{-1}). (**e**) Graph showing the percentages of podosome-rosette-positive ECs, seeded on gelatin-coated coverslips with 20 μg ml^{-1} laminin. ECs were

transduced as indicated and stimulated or not with VEGF-A for 24 h. Mean ± s.e.m. of n= 3 independent experiments in which 420 cells were analysed per experimental point. Statistical significance was calculated using a two-way ANOVA test followed by Bonferroni-adjusted *post hoc t*-tests (*P<0.05 versus its corresponding empty vector; °P < 0.05 versus empty vector L-VEGF-A−; # P < 0.05 versus empty vector L-VEGF-A+).

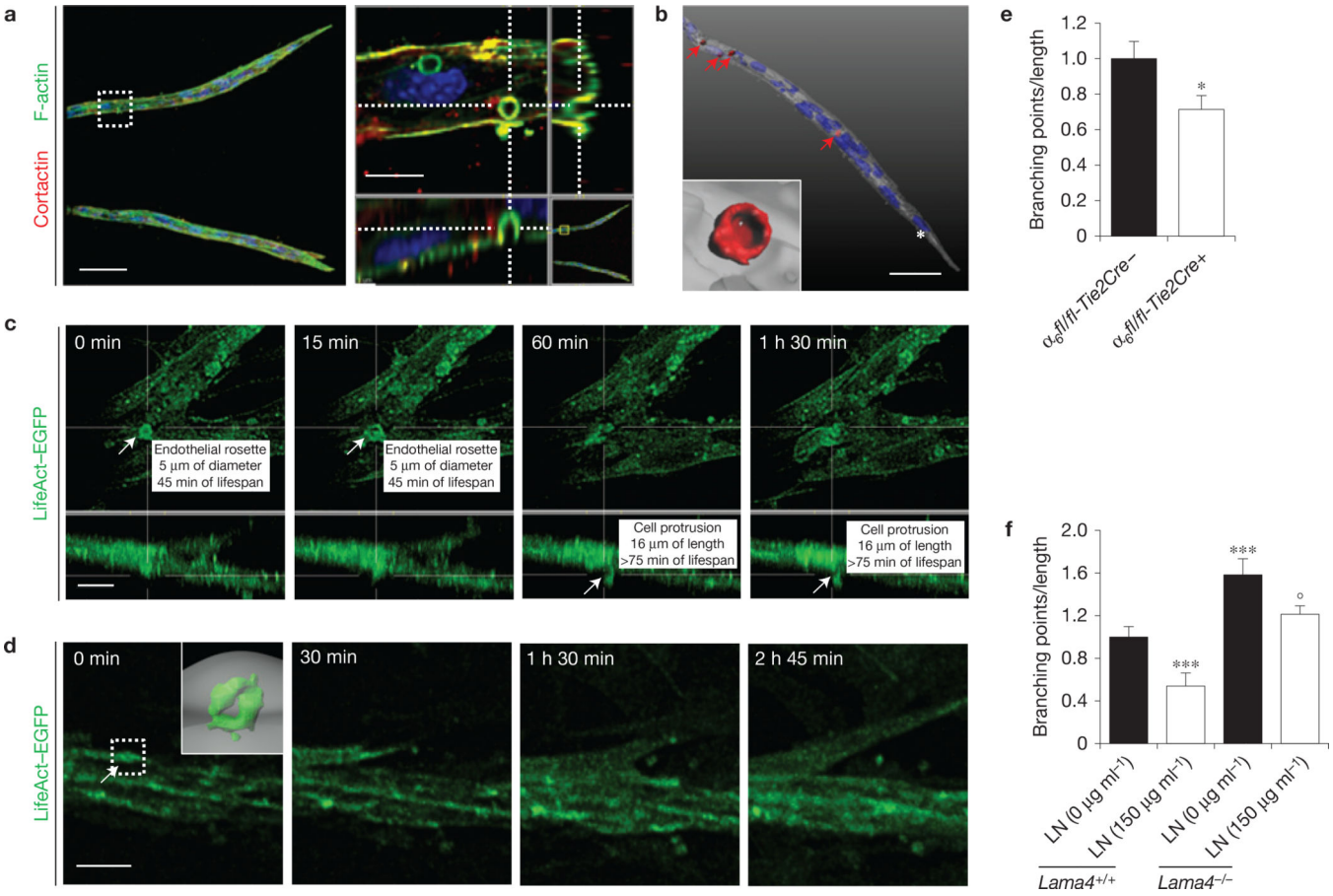

Figure 6.

Endothelial podosome rosettes precede vessel branching from a pre-existing vessel. (**a**) Confocal image stacks of representative angiogenic outgrowths from 7-day mARs into collagen gel (left panel). Scale bar, 50 μm. Right panel, *xyz*-section of the white dotted square in the left panel. Scale bar, 10μm. (**b**) 3D isosurface rendering of endothelial rosettes in angiogenic outgrowths. Angiogenic outgrowths (grey) and podosome-rosettes (red) were recognized with co-localization of F-actin/cortactin staining (indicated by red arrows) as detailed in the Supplementary Methods. The white asterisk indicates the tip-cell nucleus. Inset, a representative endothelial rosette. For complete video, see Supplementary Video 4. Scale bar, 30 μm. (**c,d**) Time-lapse multiphoton microscopy of angiogenic outgrowths from LifeAct–EGFP mARs. For complete video, see Supplementary Videos 5 and 6. The podosome rosette and cell protrusion are indicated by white arrows. Scale bar, 20 μm in **c** and 50μm in **d**. (**e**) Branching density—number of branching points divided by vascular area—of angiogenic outgrowths from WT (α_6*fl/fl-Tie2Cre*−) or endothelial α_6 null (α_6*fl/fl-Tie2Cre*+) mARs. Dynamical analysis of branching shown in Supplementary Video 7. Mean ± s.e.m. of n = 18 mARs, 3 mARs per mouse from 6 mice. Statistical significance was calculated using a two-way ANOVA test followed by Bonferroni-adjusted *post hoc t*-tests (*$P < 0.05$ versus α_6*fl/fl-Tie2Cre*−). (**f**) Branching density of angiogenic outgrowths from laminin α_4 null mARs into collagen with or without laminin addition. Dynamical analysis of *Lama4*−/− branching is shown in Supplementary Video 8 and laminin in gel in

Supplementary Video 9. Mean ± s.e.m. of n = 8 mARs, 2 mARs per mouse from 4 mice. Statistical significance was calculated using a two-way ANOVA test followed by Bonferroni-adjusted *post hoc t*-tests (***P<0.001 versus LN (0 μg ml^{-1}) WT; °P<0.05 versus LN (0 μg ml $^{-1}$) *Lama4*−/−).

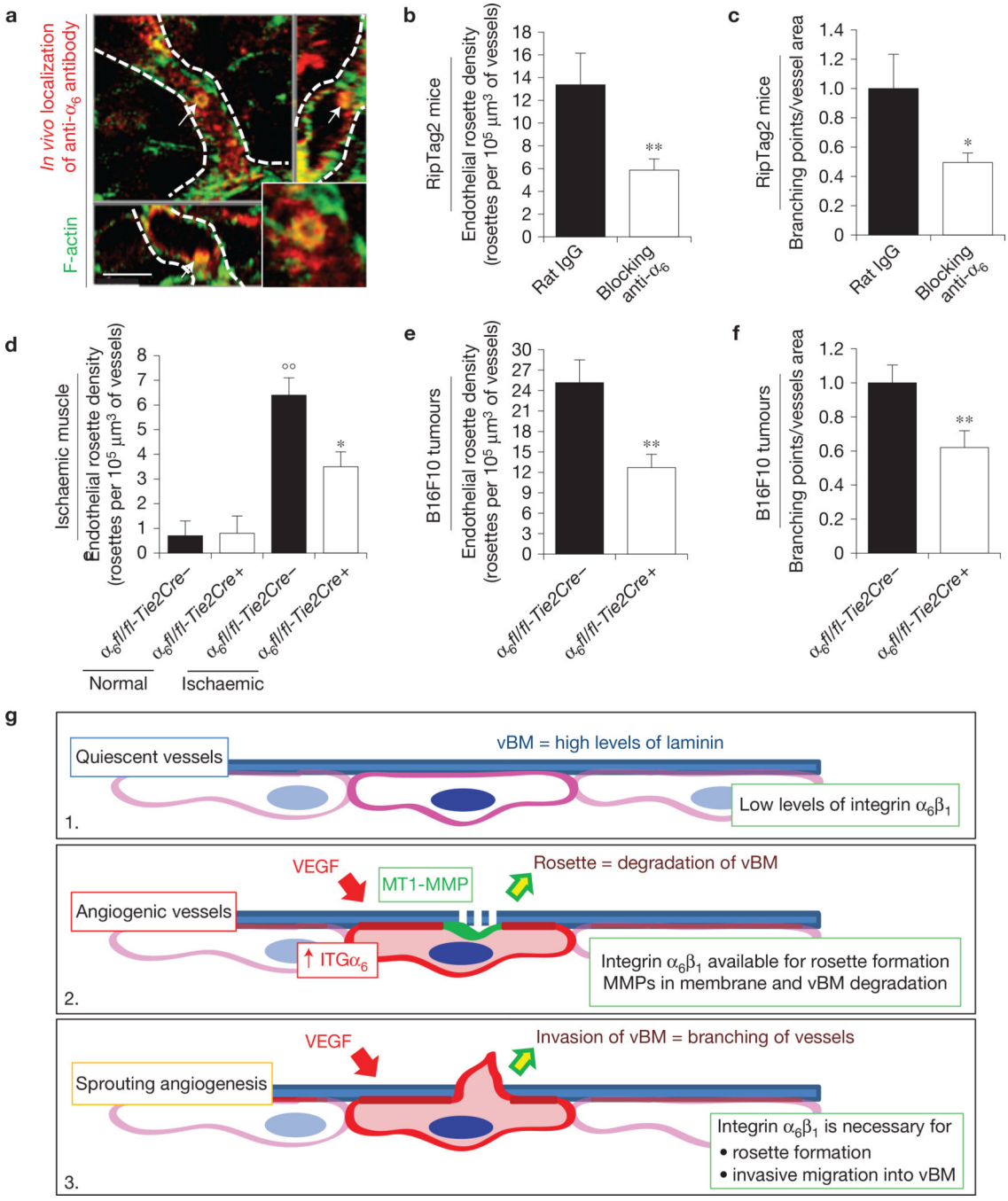

Figure 7.

In vivo blocking of integrin α_6 impairs endothelial podosome rosette formation and reduces vessel branching in tumours. (**a**) Rapid accumulation of anti-α_6 integrin antibody into endothelial podosome rosettes of RipTag2 tumour vessels. *xyz*-sections of confocal micrographs of the distribution of immunoreactivity in RipTag2 tumours 10 min after intravenous injection of 25 µg of anti-α_6 integrin antibody. Vessels are delimited by white dotted lines; white arrows indicate the podosome rosette. Inset, high magnification of the podosome rosette. Scale bar, 5 µm. (**b**) Measurements of rosette density in vessels of

RipTag2 mouse tumours, treated with rat IgG or anti-α_6 blocking antibody. Mean ± s.e.m. of n = 30 fields, 5 fields per pancreatic islet from 6 mice per treatment group. Statistical significance was calculated using an unpaired non-parametric Mann-Whitney test (**P<0.01 versus rat IgG.). (**c**) Branching density in blocking antiα_6-treated RipTag2 tumours. Mean ± s.e.m. of n = 30 fields, 5 fields per mouse from 6 mice per treatment group. Statistical significance was calculated using an unpaired non-parametric Mann-Whitney test (*P<0.05 versus rat IgG). (**d**) Measurements of rosette density in vessels of gastrocnemius muscles from unilateral hindlimb ischaemia experiments in WT (α_6*fl/fl-Tie2Cre*−) or endothelial α_6 null (α_6*fl/fl-Tie2Cre*+) mice. Mean ± s.e.m. of n = 9 fields, 3 fields per muscle from 3 mice. Statistical significance was calculated using an unpaired non-parametric Mann-Whitney test (°°P < 0.01 versus normal α_6*fl/fl-Tie2Cre*−; *P<0.05 versus α_6*fl/fl-Tie2Cre*+). (**e**) Measurements of rosette density in vessels of subcutaneous B16-F10 tumours in WT (α_6*fl/fl-Tie2Cre*−) or endothelial α_6 null (α_6*fl/fl-Tie2Cre*+) mice. Mean ± s.e.m. of n = 21 fields, 3 fields per tumour from 7 mice per treatment group. Statistical significance was calculated using an unpaired non-parametric Mann-Whitney test (**P< 0.01 versus α_6*fl/fl-Tie2Cre*−). (**f**) Branching density in B16F10 melanoma subcutaneously injected in Tie2-dependent α_6 KO mice. Mean ± s.e.m. of n = 42 fields, 5 fields per tumour from 7 mice per treatment group. Statistical significance was calculated using an unpaired non-parametric Mann-Whitney test (**P<0.01 versus α_6*fl/fl-Tie2Cre*− mice). (**g**) Cartoon showing α_6 integrin/laminin molecular mechanisms involved in sprouting angiogenesis. (1) Quiescent EC have low levels of $\alpha_6\beta_1$ integrin, which binds vBM laminin, is recruited in FAs, and results in blood vessel stabilization. (2) When the tumour produces VEGF, the VEGF induces upregulation of the α_6 integrin subunit in ECs. The increased availability of $\alpha_6\beta_1$ integrin then allows the formation and stabilization of endothelial podosome rosettes and the ensuing MMP-driven degradation of ECM that, in turn, (3) allows vBM invasion by ECs and sprouting angiogenesis.